Supporting Information

Biomimetic Modeling of Copper Nitrite Reductase: Acid-Catalyzed Reduction of Nitrite to Nitric Oxide at Cu(I)-center via a Cu(II)-hydroxide Intermediate

Prabhakar Bhardwaj, Sanjai Muthusamy, Soumyadip Ray, Padmabati Mondal, and Pankaj Kumar*

Department of Chemistry, Indian Institute of Science Education and Research (IISER) – Tirupati, Tirupati, 517619, India

* To whom correspondence should be addressed.

E-mail: pankajatiisert@gmail.com, pankaj@iisertirupati.ac.in

Table of Contents

Experimental Section

Materials. All reagents and solvents obtained from commercial sources (Sigma Aldrich Chemical Co. and Tokyo Chemical Industry) were of the best available purity and used without further purification unless otherwise indicated. Solvents were dried according to the reported literature and distilled under an inert atmosphere before use.[S1] $Na^{15}NO_2$ (99.2% ^{15}N-enriched) was purchased from ICON Services Inc. (Summit, NJ, USA). The PMDTA ligand (*N*,*N*,*N*′,*N*′,*N*″-Pentamethyl-diethylenetriamine) was purchased from Sigma Aldrich and distilled before use. The 12-TMC ligand was prepared by reacting excess amounts of formaldehyde and formic acid with 1,4,7,10-tetraazacyclododecane as reported previously.[S2]

Instrumentation. Electronic absorption spectra were recorded on an Agilent Technologies Cary 8454 diode-array spectrometer equipped with a thermostat cell holder (UNISOKU Scientific Instruments) designed for low-temperature experiments. FT-IR spectra in solid form were recorded on a Bruker-Alpha Eco-ATR FTIR spectrometer using the standard KBr disk method. The FT-IR spectra were recorded on the Bruker-Alpha Eco-ATR FTIR spectrometer using the KBr disk method. ^{1}H-NMR spectra were measured with a Bruker model Ascend 400 FT-NMR spectrometer. Electrospray ionization mass spectra (ESI-MS) were recorded on an Agilent Mass Spectrometer (6200 series TOF/6500 series Q-TOF B.08.00) by infusing samples directly into the source using a manual method. The spray voltage was set at 4.2 kV and the capillary temperature at 80 °C. NO gas detection was performed by headspace Mass spectrometry using an online MS with an OmniStarTM Gas Analysis System GSD 320 (Pfeiffer) quadrupole mass spectrometer. Single crystal X-ray diffraction data were collected using a Bruker D8 Venture Super Duo diffractometer with a Photon-III detector using a Mo source (λ = 0.71073 Å). Electron Paramagnetic Resonance (EPR) spectroscopy was studied using a Bruker spectrometer (Bruker, EMXmicro) operating at an X-band frequency (Microwave frequency: 9.31 GHz) and a magnetic field modulation of 100 kHz, with a microwave power of 48.83 mW and a modulation amplitude of 10 G at 100 K. Electrochemical measurements (cyclic voltammetry) were performed at 298 K using an CH Instruement Electrochemical analyser in distilled and degassed acetonitrile containing $TBAPF_6$ (tetrabutylammonium n hexafluorophosphate, 0.10 M) as a supporting electrolyte under Ar. A conventional three-electrode cell was used with a glassy carbon working electrode and a platinum wire as a counter electrode. The measured potentials were recorded with respect to SCE.

Synthesis of [PMDTA)Cu^{I}(CH$_3$CN)](ClO$_4$) (1). A CH_3CN solution (3 mL) of $[Cu^{I}(CH_3CN)_4](ClO_4)$ (327.2 mg, 1.0 mmol) was added to a 5 mL CH_3CN solution of PMDTA (173.3 mg, 1.0 mmol) with constant stirring for 1 hour at 298K in an argon atmosphere. The color of the solution remains colorless. After the reaction was complete, the reaction mixture was reduced under reduced pressure, and diethyl ether was added to precipitate the white complex **1.** Further, **1** was layered with diethyl ether and kept for crystallization at 298 K. Colorless crystals were obtained in 3-4 days. Yield: 339 mg (~ 90%). Electronic absorption: No *d-d* band was observed. FT-IR (KBr pellet): 2900, 1625, 1454, 1095 cm^{-1}.

Synthesis of [(PMDTA)Cu^{I}(NO$_2^-$)] (2). To a 5.0 mL CH_3CN solution of $[PMDTA)Cu^{I}(CH_3CN)](ClO_4)$ (**1**) (188.65 mg, 0.5 mmol), 1 mL solution of $NaNO_2$ (34.5 mg, 1.0 equivalent) with 15-crown-5 (2.5 equivalents) was added slowly with constant stirring in an argon atmosphere. The reaction mixture changes from colorless to light yellow. The mixture was stirred for 1 hour at 298 K. The volume of the reaction mixture was decreased to 1.0 mL under reduced pressure and then layered with diethyl ether and kept for crystallization at 298 K. Light yellow color crystals were obtained in 2-3 days. Yield: 242 mg (~ 92%). Electronic absorption: λ_{max} = 365 nm (ε = 160 M^{-1} cm^{-1}). FT-IR (KBr pellet): 2910, 1471, 1625, 1270, 1095 cm^{-1}.

Synthesis of [(PMDTA)Cu^{I}(^{15}NO$_2^-$)] (2-^{15}NO$_2^-$). To a 5.0 mL CH_3CN solution of $[PMDTA)Cu^{I}(CH_3CN)](ClO_4)$ (**1**) (189.0 mg, 0.5 mmol), 1 mL solution of $^{15}NaNO_2$ (35 mg, 0.5 mmol) with 15-crown-5 (2.5 equivalents) was added slowly with constant stirring in an argon atmosphere. The color of the reaction mixture changes from colorless to light yellow. The mixture was stirred for 1 hour at 298 K. Upon completion of the reaction, the complex was precipitated with diethyl ether. Yield: 238 mg (~ 90%). FT-IR (KBr pellet): 2910, 1471, 1625, 1246, 1095 cm^{-1}.

Reactivity studies. All Electronic absorption spectral measurements were performed in a cuvette in CH_3CN under Ar at different temperatures as required by the reaction. All kinetic reactions were conducted at least three times, and the data reported here represent the average outcome of these reactions. We have performed all reactions in degassed solutions under Argon (glove box) to avoid dioxygen interaction or reaction with nitrosyl or nitric oxide (NO). The formation of the $\{CoNO\}^8$ complex above nitrite reduction reactions was confirmed by comparison with authentic samples, and product yields were determined by comparison with standard curves prepared using the original samples.

Reactivity of [(PMDTA)Cu^{I}(NO_2^-)] (2) + Two equivalent of Acid ($HClO_4$, H^+): Formation of complex 3. Complex **2** was reacted with the two equivalents of perchloric acid ($HClO_4$) in CH_3CN under an Argon atmosphere at 298 K. The color of the above reaction mixture changed from light yellow to blue upon the addition of two equivalents of H^+, indicating the formation of **3**. The product obtained in the reaction of **2** and two equivalents of H^+ was compound **3**, and confirmed with the help of various spectroscopic and structural characterizations using SCXRD. Electronic absorption: λ_{max} = 605 nm (ε = 220 M^{-1} cm^{-1}). FT-IR (KBr pellet): 2915, 1628, 1471, 1095 cm^{-1}. Electrospray ionization mass spectrum (ESI-MS) of **3** showed prominent peaks at m/z = 335.1 (calc. m/z = 335.1), 281.1 (calc. m/z = 281.1), and 491.3 (marked with a blue asterisk, calc. m/z = 271.1), and their mass and isotopic distribution pattern correspond to [(PMDT)Cu^{II}(ClO_4)]$^+$, [(PMDT)Cu^{II}(HCOO)]$^+$, and [(PMDT)Cu(CH_3OH)(H_2O]$^+$, respectively.

Magnetic moment calculation and determination of the spin-state of Cu-center in complexes 3: Evans' method of ^{1}H-NMR was performed to determine the spin state (number of unpaired electrons) of Cu-center in **3** at 298 K. A WILMAD® coaxial insert (with a sealed capillary) tubes containing only CD_3CN solvent (with 1.0% TMS) were inserted into the standard NMR tubes containing the **3** (4.0 mM, with 1.0% TMS), respectively.[S3] We have calculated the chemical shift values of the TMS peak in the presence of **3** with respect to those of the TMS peak in the outer NMR tube. The magnetic moments for both complexes were calculated using the given equation.

3

$$\mu_{eff} = 0.0618(\Delta \nu T/2fM)^{1/2}$$

$$\mu_{eff} = 0.0618(8 \times 298 / 2 \times 400 \times 0.004)^{1/2}$$

$$\mu_{eff} = 1.70 \text{ BM}$$

Reactivity of [(PMDTA)Cu^{I}(NO_2^-)] (2) + one equivalent of Acid ($HClO_4$, H^+). To explore the formation of the intermediate, Complex **2** was reacted with the slow addition of one equivalent of perchloric acid ($HClO_4$) in CH_3CN under an Argon atmosphere at 233 K, and the Electronic absorption spectrum indicated the formation of an intermediate species. This was further characterized with EPR and IR, which confirmed the formation of {Cu^{II}-OH}$^+$ as the intermediate. Electronic absorption: λ_{max} = 389 nm (ε = 160 M^{-1} cm^{-1}). EPR: g = 2.15. FT-IR (KBr pellet): 3615, 2914, 1628, 1471, 1095 cm^{-1}.

Trapping of NO with [(12-TMC)Co^{II}]$(BF_4)_2$ (Qualitative and quantitative Estimation). Complex [(12-TMC)Co^{II}]$(BF_4)_2$ was used as a trapping agent of NO in the reaction of **2** with acid. For qualitative estimation, a small culture vial containing a solution of **2** (40 mM) in argon-saturated CH_3CN was placed in a larger vial with a solution of [(12-TMC)$Co^{II}(CH_3CN)](BF_4)_2$ (40 mM) in argon-saturated CH_3CN. The larger vial was sealed with the septum. A solution of $HClO_4$ (two equivalents, 80 mM) in Argon-saturated CH_3CN was injected into the inner vial. The solution was stirred for 4 hours, and the complete setup was then left at 273 K for 12 hours. The inner sample vial was removed, and the product in the outer sample vial was then precipitated out using diethyl ether. Further, the product was characterized using different spectroscopic methods, confirming the formation of [(12-TMC)Co(NO)]$(BF_4)_2$, which was produced by the reaction of [(12-TMC)$Co^{II}(CH_3CN)](BF_4)_2$ with NO released from **2** in the presence of acid (Figure S7a-c). Characterization of $\{CoNO\}^8$ isolated from the above reaction (outer sample vial): Electronic absorption: λ_{max} = 370 nm and 535, FT-IR (KBr pellet): 2931, 1703, 1465, 1100 cm^{-1}.

For the quantitative estimation of NO formed in the above reaction, complex **2** (0.5 mM) in a small vial and [(12-TMC)$Co^{II}(CH_3CN)](BF_4)_2$ (0.5 mM) in an outer vial (as per the above reaction conditions) were prepared in the glove box. Two equivalents of acid were added to the inner sample vial containing **2**, and the reaction setup was maintained for 12 hours. The electronic absorption spectrum of $\{CoNO\}^8$ was recorded and compared with the authentic sample. The quantification of $\{CoNO\}^8$, formed in the above experiment, was done by comparing the molar extinction coefficient of $\{CoNO\}^8$ (λ = 370 nm) with that of the authentic sample. The yield of $\{CoNO\}^8$ was determined to be ~86% based on the calculation shown below (Figure S7d).

Trial	*Absorbance of Authentic $\{CoNO\}^8$ (A)*	*Absorbance of Trapped $\{CoNO\}^8$ in the reaction of **2** with two equivalents of H^+ and trapped with the Trapping reagent. (B)*	*Ratio of (B/A) = C*	*% Yield (C *100)*
1	*0.38*	*~0.33*	*0.86*	*86*
2	*0.38*	*~0.32*	*0.84*	*84*
3	*0.38*	*~0.34*	*0.89*	*89*
			Average Yield	***86.3 = ~86***

Similarly, the quantification of $\{CoNO\}^8$ was performed by comparing the molar extinction coefficient of the trapped $\{CoNO\}^8$, formed in the reaction of **2** (0.5 mM) with one equivalent of H^+ and [(12-TMC)$Co^{II}(CH_3CN)](BF_4)_2$ (0.5 mM), as per the above experimental setup, with

that of the authentic {CoNO}^{8}. The yield of {CoNO}^{8} was determined to be ~80% based on the calculation shown below (Figure S8).

Trial	*Absorbance of Authentic {CoNO}^{8} (A)*	*Absorbance of Trapped {CoNO}^{8} in the reaction of **2** with one equivalent of H^+ and trapped with the Trapping reagent. (B)*	*Ratio of (B/A) = C*	*% Yield (C *100)*
1	*0.38*	*~0.30*	*0.79*	*79*
2	*0.38*	*~0.31*	*0.81*	*81*
3	*0.38*	*~0.30*	*0.79*	*79*
		Average Yield		***79.6 = ~80***

^{15}N-labeling experiments (following the N-atom by FT-IR): We have recorded the IR spectra of the different complexes in their solid form as a KBr pellet to follow the source of N-atom ($^{14/15}$N). The IR spectra of complexes **2** showed a nitrite ($^{14}NO_2^-$) characteristic peak at 1270 cm^{-1}, which shifted to 1246 cm^{-1} when prepared with ^{15}N-labeled nitrite ($^{15}NO_2^-$). The change in the IR stretching frequency of copper-bound NO_2^- (Δ = 24 cm^{-1}) confirmed that an increase in the reduced mass of the nitrogen atom (^{14}N to ^{15}N) is responsible for the decrease in the stretching frequency of the NO_2^- functional group. As the To follow the $NO_{(g)}$ generated in the Cu^I- NO_2^- reduction reaction, we have used our previously reported Co-12TMC complex to trap $NO_{(g)}$ as cobalt-nitrosyl complex ({CoNO}^{8}).[S4] We observed similar spectral shift/changes as observed for **2**-$^{14/15}NO_2^-$ complexes when the IR spectra were recorded for trapped {CoNO}^{8} in the acid-induced NO_2^--reduction (^{14}N and ^{15}N-labeled NO_2^-) in complex **2**. The IR spectra of {CoNO}^{8} showed a characteristic nitrosyl stretching frequency at 1703 cm^{-1} (^{14}N), which shifted to 1670 cm^{-1} (Δ = 33 cm^{-1}) upon exchange with the ^{15}N-labeled nitrosyl functional group.

NO gas detection by headspace Mass spectrometry: We detected the $NO_{(g)}$ ($^{14}NO/^{15}NO$) formed in the reaction of **2** with acid ($HClO_4$) using an online MS with an OmniStar^{TM} Gas Analysis System GSD 320 (Pfeiffer) quadrupole mass spectrometer apparatus. To follow the $NO_{(g)}$ generated in the NO_2^- reduction, a sample vial (5.0 mL) containing a CH_3CN solution of **2** (5.0 Mm, 2.0 mL) sealed with a rubber septum was taken from the glove box and attached to the capillary from mass spectrometry into the headspace of the sealed vial for real-time measurement. $HClO_4$ (10 mM) solution was prepared in CH_3CN in other sample vials inside the glove box. Two equivalents of $HClO_4$ (100 µl, 10 mM) were added to the solution of **2** using a gas-tight Hamilton syringe, piercing through the rubber septum. The reactions were

kept for 10 minutes at RT (298 K) before analyzing the target gases ($^{14}NO/^{15}NO$). We observed the formation of ^{14}NO and ^{15}NO gases.

Single-Crystal XRD Studies. Crystals were mounted on Hampton cryoloops. All geometric and intensity data for the crystals were collected using a Bruker D8 Venture super Duo diffractometer with Photon-III detector using Mo source diffractometer equipped with a micro-focus sealed X-ray tube Mo-Kα (λ = 0.71073 Å) X-ray source and HyPix3000 (CCD plate) detector of with increasing ω (width of 0.3 per frame) at a scan speed of either 5 or 10 s/frame. The CrysAlisPro software was used for data acquisition and data extraction. Using Olex2[S6], the structure was solved with the SIR2004[S5,S6,S7] structure solution program using Direct Methods and refined with the ShelXL[S8] refinement package using Least Squares minimization. All non-hydrogen atoms were refined with anisotropic thermal parameters. Detailed crystallographic data and structural refinement parameters are summarized in Tables T1–T5. The CCDC numbers for complexes 1, 2, and 3 are 2496916, 2496918 & 2496918, respectively.

Nitric Oxide Preparation and Purification. NO was prepared and purified by following a detailed procedure, as shown in Fig. S7. First, NO gas was prepared by reacting $NaNO_2$ with H_2SO_4 under an Ar atmosphere and then passed through two different types of columns. First, pass through a column packed with NaOH beads to remove higher-nitrogen-oxide impurities. After that, the gas passes through two columns filled with NaOH beads and molecular sieves to remove the minor amount of remaining higher nitrogen oxides and moisture impurities. The highly purified NO gas was then collected in a vacuum Schlenk flask fitted with a rubber septum (free from oxygen; after several vacuum and Ar purging). High-pressure NO gas (with pressure >1 atmosphere; the septum bulges outward due to high pressure) then passed through an Ar-saturated (oxygen-free) and dry Acetonitrile (CH_3CN) solution for 15 minutes. The concentration of NO in the NO-saturated CH_3CN solution is ~14 mM.[S9]

Water Content Determination (Karl Fischer Titration). The water content in the reaction of **2** with 2 equivalents of H^+ was determined using a Metrohm Ecoscan Coulometer equipped with a generator electrode. All measurements were carried out under a dry Ar-purged atmosphere to prevent contamination by atmospheric moisture. Instrument performance was verified using a certified Hydranal Water Standard prior to analysis.

For each measurement, the sample was introduced into the titration cell using a 1 mL gas-tight Hamilton syringe through the septum. The sample mass was determined by difference weighing using an analytical balance with a precision of ±0.0001 g. The sample amount was

optimized to ensure that the water content remained within the optimal detection range of the coulometric titration.

The water content was calculated automatically by the instrument. Each measurement was performed in **triplicate** to ensure reproducibility. The average water content increased from 3.06 μg to 5.76 μg (Δ = 3.70 μg) upon treatment with two equivalents of H+, with consistent results across three independent measurements.

Sample S.No.	***Amount of water detected in 2 (μg)***	***Amount of water detected in reaction 2 + H^+ (μg)***
1	*3.2*	6.7
2	*3.0*	6.9
3	*3.0*	6.7
Average	***3.06***	6.76

DFT Calculation: We have optimized the cations of the reactant and intermediate using the B3LYP functional [S10,S11,S12] and Def2-TZVP basis set[S13] in the gas phase. In this calculation, we have used Grimme's DFT empirical dispersion correction (GD3BJ).[S14] The frequency calculation confirms that the molecules have reached local minima, as no imaginary frequencies are observed. Later, we obtained the optimized structures using the M06 functional[S15] and the Def2-TZVP basis set in an acetonitrile medium. Solvent effect has been taken into account using the continuum solvent model of SMD in acetonitrile.[S16] The vibrational analysis provides the thermochemical insight. All calculations are done in Gaussian 09 software.[S17]

References:

S1. Armarego, W. L. F.; Chai, C. L. L., *Purification of Laboratory Chemicals*, 6th ed.; Pergamon Press: Oxford, **2009**.

S2. Halfen, J. A.; Young, V. G., Jr. Efficient Preparation of 1,4,8-trimethylcyclam and its Conversion into a Thioalkyl-pendant Pentadentate Chelate. *Chem. Commun*. **2003**, 2894.

S3. Evans, D. F., 400. The determination of the paramagnetic susceptibility of substances in solution by nuclear magnetic resonance. *J. Chem. Soc*. 1959, 2003-2005

S4. Kumar, P.; Lee, Y. M.; Park, Y. J.; Siegler, M. A.; Karlin, K. D.; Nam, W., Reactions of Co(III)-nitrosyl complexes with superoxide and their mechanistic insights. *J. Am. Chem. Soc.* **2015**, 137, 4284-4287.

S6. Dolomanov, O. V.; Bourhis, L. J.; Gildea, R. J.; Howard, J. A. K.; Puschmann, H., OLEX2: a Complete Structure Solution, Refinement and Analysis Program. *J. Appl. Cryst*. **2009**, *42*, 339–341.

S7. Burla, M. C.; Caliandro, R.; Camalli, M. C., B.; Cascarano, G. L.; De Caro, L.; Giacovazzo, C.; Polidori, G.; Siliqi, D.; Spagna, R., IL MILIONE: A Suite of Computer Programs for Crystal Structure Solution of Proteins. *J. Appl. Cryst.* **2007**, *40*, 609–613.

S8. Sheldrick, G. M., Crystal Structure Refinement with SHELXL. *Acta Cryst*. **2015**, *C71*, 3–8.
S9. Young, C. L., Solubility Data Series Val. 8 Oxides of Nitrogen, *International Union of Pure and Applied Chemistry* (IUPAC). **1981**.
S10. Becke, A. D., Density-functional exchange-energy approximation with correct asymptotic behavior. *Phys. Rev. A.* 1988, 38, 3098.
S11. Lee, C.; Yang, W.; Parr, R. G., Development of the Colle-Salvetti correlation-energy formula into a functional of the electron density. *Phys. Rev. B.* **1988**, 37, 785.
S12. Becke, A. D., Density-functional thermochemistry. III. The role of exact exchange. *J. Chem. Phys.* **1993**, 98, 5648.
S13. Weigend, F.; Alrichs, R., Balanced basis sets of split valence, triple zeta valence and quadruple zeta valence quality for H to Rn: Design and assessment of accuracy. *Phys. Chem. Chem. Phys.*, **2005**,7, 3297-3305.
S14. Grimme, S.; Ehrlich, S.; Goerigk, L., Effect of the damping function in dispersion-corrected density functional theory. J. Comput. Chem. 2011, 32, 1456–1465.
S15. Zhao, Y.; Truhlar, D. G., The M06 suite of density functionals for main group thermochemistry, thermochemical kinetics, noncovalent interactions, excited states, and transition elements: two new functionals and systematic testing of four M06-class functionals and 12 other functionals. *Theor. Chem. Account*. **2008**, 120, 215–241.
S16. Marenich, A. V.; Cramer, C.J.; Truhlar, D. G., Universal Solvation Model Based on Solute Electron Density and on a Continuum Model of the Solvent Defined by the Bulk Dielectric Constant and Atomic Surface Tensions. *J. Phys. Chem. B.* **2009**, 113, 18, 6378–6396.
S17. Gaussian 09, Revision D.01: Frisch, M. J.; Trucks, G. W.; Schlegel, H. B.; Scuseria, G. E.; Robb, M. A.; Cheeseman, J. R.; Scalmani, G.; Barone, V.; Mennucci, B.; Petersson, G. A.; Nakatsuji, H.; Caricato, M.; Li, X.; Hratchian, H. P.; Izmaylov, A. F.; Bloino, J.; Zheng, G.; Sonnenberg, J. L.; Hada, M.; Ehara, M.; Toyota, K.; Fukuda, R.; Hasegawa, J.; Ishida, M.; Nakajima, T.; Honda, Y.; Kitao, O.; Nakai, H.; Vreven, T.; Montgomery, J. A., Jr.; Peralta, J. E.; Ogliaro, F.; Bearpark, M.; Heyd, J. J.; Brothers, E.; Kudin, K. N.; Staroverov, V. N.; Kobayashi, R.; Normand, J.; Raghavachari, K.; Rendell, A.; Burant, J. C.; Iyengar, S. S.; Tomasi, J.; Cossi, M.; Rega, N.; Millam, J. M.; Klene, M.; Knox, J. E.; Cross, J. B.; Bakken, V.; Adamo, C.; Jaramillo, J.; Gomperts, R.; Stratmann, R. E.; Yazyev, O.; Austin, A. J.; Cammi, R.; Pomelli, C.; Ochterski, J. W.; Martin, R. L.; Morokuma, K.; Zakrzewski, V. G.; Voth, G. A.; Salvador, P.; Dannenberg, J. J.; Dapprich, S.; Daniels, A. D.; Farkas, Ö.; Foresman, J. B.; Ortiz, J. V.; Cioslowski, J.; Fox, D. J., Gaussian, Inc., Wallingford CT, 2009.

Table ST1: Crystallographic data for **1**.

Empirical formula	$C_{11}H_{26}ClCuN_4O_4$
Formula weight	377.35
Temperature/K	150.00
Crystal system	triclinic
Space group	P1
a/Å	7.3803(7)
b/Å	7.4795(7)
c/Å	8.8543(8)
α/°	87.186(3)
β/°	77.327(4)
γ/°	63.600(3)
Volume/Å3	426.47(7)
Z	1
ρcalcg/cm3	1.469
μ/mm-1	1.456
F(000)	198.0
Radiation	MoKα (λ = 0.71073)
2Θ range for data collection/°	4.722 to 56.74
Index ranges	$-9 \leq h \leq 9$, $-9 \leq k \leq 9$, $-11 \leq l \leq 11$
Reflections collected	14467
Independent reflections	4150 [Rint = 0.0341, Rsigma = 0.0417]
Data/restraints/parameters	4150/3/191
Goodness-of-fit on F2	1.037
Final R indexes [I>=2σ (I)]	R1 = 0.0393, wR2 = 0.1081
Final R indexes [all data]	R1 = 0.0399, wR2 = 0.1087
Largest diff. peak/hole / e Å-3	1.07/-0.81

Table ST2: Crystallographic data for **2**.

Empirical formula	$C_{38}H_{79}Cl_2Cu_2N_8Na_2O_{22}$
Formula weight	1244.05
Temperature/K	150.00
Crystal system	triclinic
Space group	P-1
a/Å	13.2220(10)
b/Å	14.9599(10)
c/Å	16.7372(12)
α/°	66.145(2)
β/°	88.810(3)
γ/°	75.469(3)
Volume/Å^3	2918.7(4)
Z	2
ρ_{calc}g/cm^3	1.416
μ/mm^{-1}	0.912
F(000)	1306.0
Radiation	MoKα (λ = 0.71073)
2Θ range for data collection/°	3.14 to 56.772
Index ranges	$-17 \leq h \leq 17$, $-19 \leq k \leq 20$, $-22 \leq l \leq 22$
Reflections collected	105077
Independent reflections	14485 [R_{int} = 0.0741, R_{sigma} = 0.0531]
Data/restraints/parameters	14485/707/797
Goodness-of-fit on F^2	1.041
Final R indexes [I>=2σ (I)]	R_1 = 0.0606, wR_2 = 0.1612
Final R indexes [all data]	R_1 = 0.0812, wR_2 = 0.1804
Largest diff. peak/hole / e Å^{-3}	1.57/-1.04

Table ST3: Crystallographic data for **3**

Empirical formula	$C_{13}H_{29}Cl_2CuN_5O_8$
Formula weight	517.85
Temperature/K	298.00
Crystal system	monoclinic
Space group	P21/c
a/Å	8.5452(12)
b/Å	17.312(2)
c/Å	15.8338(19)
α/°	90
β/°	96.835(6)
γ/°	90
Volume/Å3	2325.8(5)
Z	4
ρcalcg/cm3	1.479
μ/mm-1	1.215
F(000)	1076.0
Radiation	MoKα (λ = 0.71073)
2Θ range for data collection/°	3.5 to 50.7
Index ranges	$-10 \leq h \leq 10$, $-20 \leq k \leq 20$, $-19 \leq l \leq 19$
Reflections collected	73023
Independent reflections	4268 [Rint = 0.0998, Rsigma = 0.0353]
Data/restraints/parameters	4268/0/269
Goodness-of-fit on F2	1.053
Final R indexes [I>=2σ (I)]	R1 = 0.0467, wR2 = 0.1268
Final R indexes [all data]	R1 = 0.0536, wR2 = 0.1333
Largest diff. peak/hole / e Å-3	0.69/-0.36

Table ST4: Selected bond lengths (Å) and bond angles (°) for **1** and **2**.

1		**2**	
Cu1 N1	2.086(4)	N1 O1	1.252(4)
Cu1 N2	2.181(4)	N1 O2	1.244(4)
Cu1 N3	2.160 (4)	Cu1 N1	1.933(3)
Cu1 N4	1.900(4)	Cu1 N2	2.103(3)
O1 Cl1	1.393(12)	Cu1 N3	2.107(3)
O2 Cl1	1.377(13)	Cu1 N4	2.178(3)
O3 Cl1	1.414(5)	Cu2 N5	1.934(3)
O4 Cl1	1.4374(5)	Cu2 N6	2.096(3)
N1 Cu1 N2	85.61(14)	O2 N1 O1	115.3(3)
N1 Cu1 N3	118.90(15)	O1 Cu1 N1	118.6(2)
N1 Cu1 N4	126.59(16)	N1 Cu1 N3	125.55(12)
N4 Cu1 N2	124.89(16)	N1 Cu1 N4	114.98(12)
N4 Cu1 N3	107.34(16)	N1 Cu1 N2	115.48(13)
N2 Cu1 N3	85.50(14)	N3 Cu1 N4	84.78(12)
C1 Cu1 N1	109.7(3)	N2 Cu1 N3	115.98(12)
C3 N1 Cu1	105.3(3)	N2 Cu1 N4	86.39(12)

Table ST5: Selected bond lengths (Å) and bond angles (°) for **3**.

3	
Cu1 O1	1.996(2)
Cu1 N1	1.990(3)
Cu1 N2	2.038(3)
Cu1 N3	2.050 (3)
Cu1 N4	2.194(3)
O1 N5	1.289(4)
O2 N5	1.230(4)
Cu1 O2	2.650(2)
N1 Cu1 O1	94.55(11)
N1 Cu1 N2	81.37(12)
N1 Cu1 N3	165.89(12)
N1 Cu1 N4	108.07(12)
N2 Cu1 O1	164.23(11)
N3 Cu1 O1	92.32(11)
N4 Cu1 O1	95.49(11)
N2 Cu1 N4	103.43(11)
N2 Cu1 N3	86.37(12)
O2 N5 O1	114.2(3)

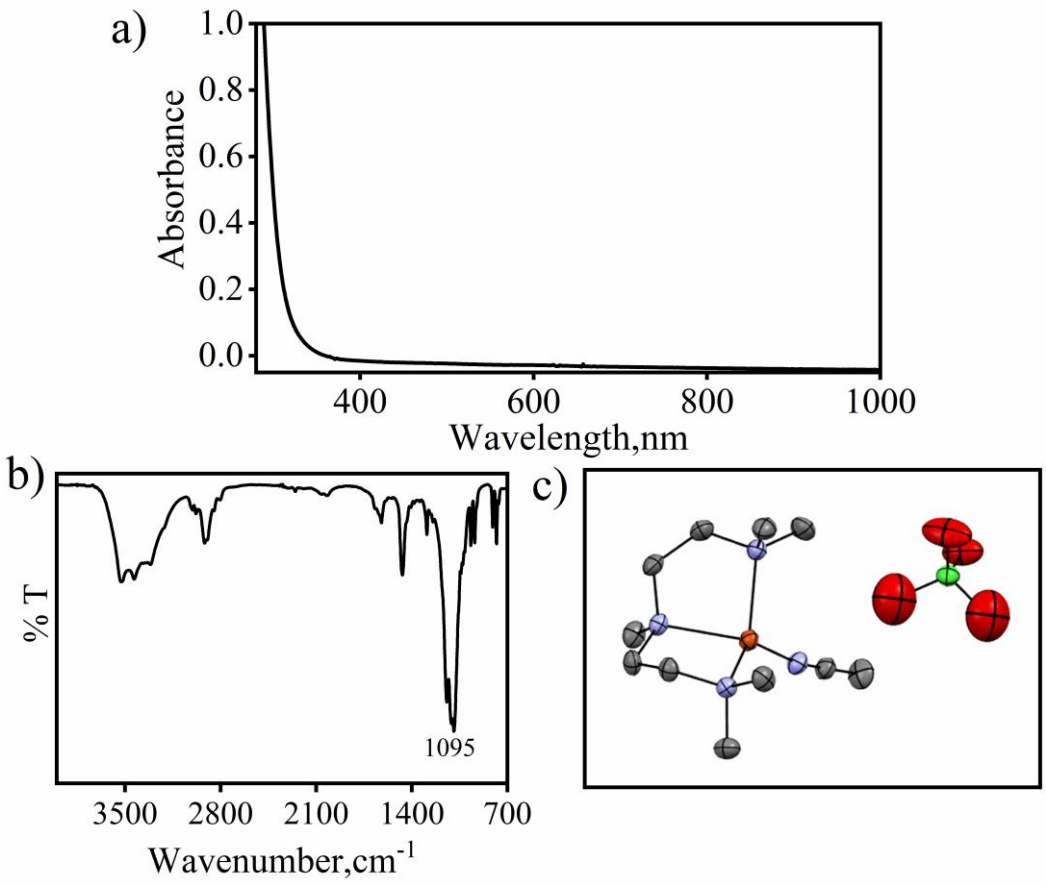

Figure S1. (a) Electronic absorption spectra of **1** (0.5mM) in CH_3CN at 298 K. (b) FT-IR spectrum of **1** recorded in a KBr pellet at 298 K. (c) Displacement ellipsoid plots (50% probability level) of **1.** Hydrogen atoms are removed for better clarity. (Orange: Cu, Blue: N, Grey: C, Green: Cl, Red: O)

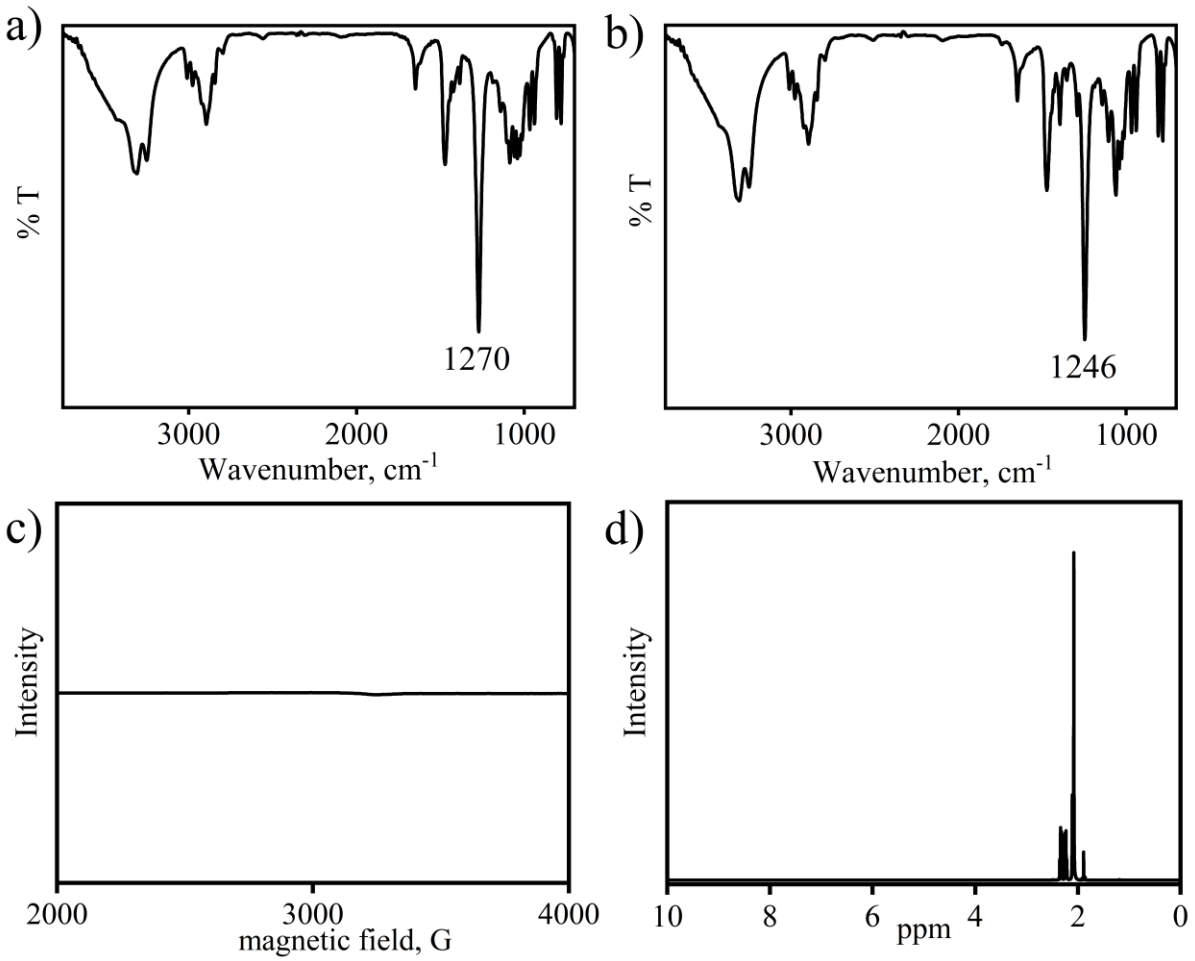

Figure S2. (a) FT-IR spectrum of **2** recorded in a KBr pellet at 298 K, showing the peaks for **2**-$^{14}NO_2^-$ (1270 cm^{-1}). (b) FT-IR spectra of **2**-$^{15}NO_2^-$ (1246 cm^{-1}) recorded in KBr pellet at 298 K. (c) EPR spectrum of **2** at 100 K. (d) ^{1}H-NMR (400 MHz) spectra of **2** (10 mM) in CD_3CN at 298 K.

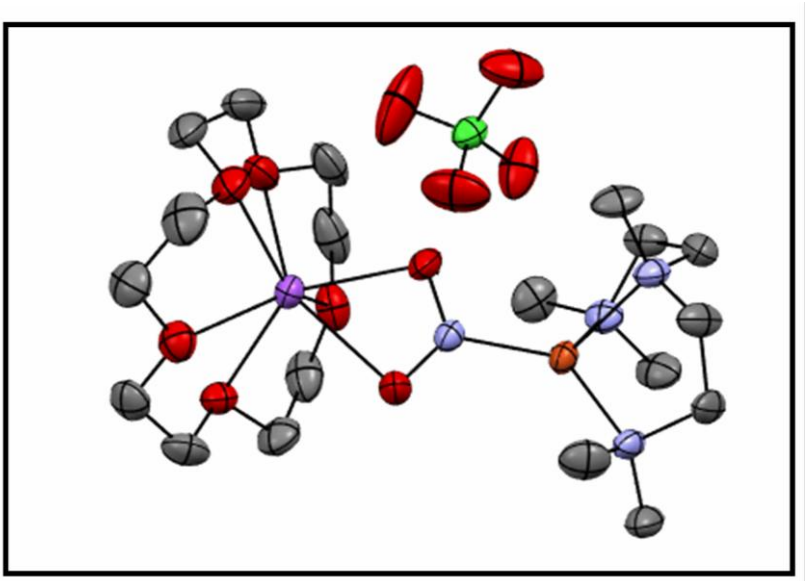

Figure S3. Displacement ellipsoid plots (50% probability level) of **2** grown in the reaction of **1** with one equivalent $NaNO_2$ and 15-crown-5. Hydrogen atoms are removed for better clarity. (Orange: Cu, Blue: N, Grey: C, Green: Cl, Red: O, Purple: Na)

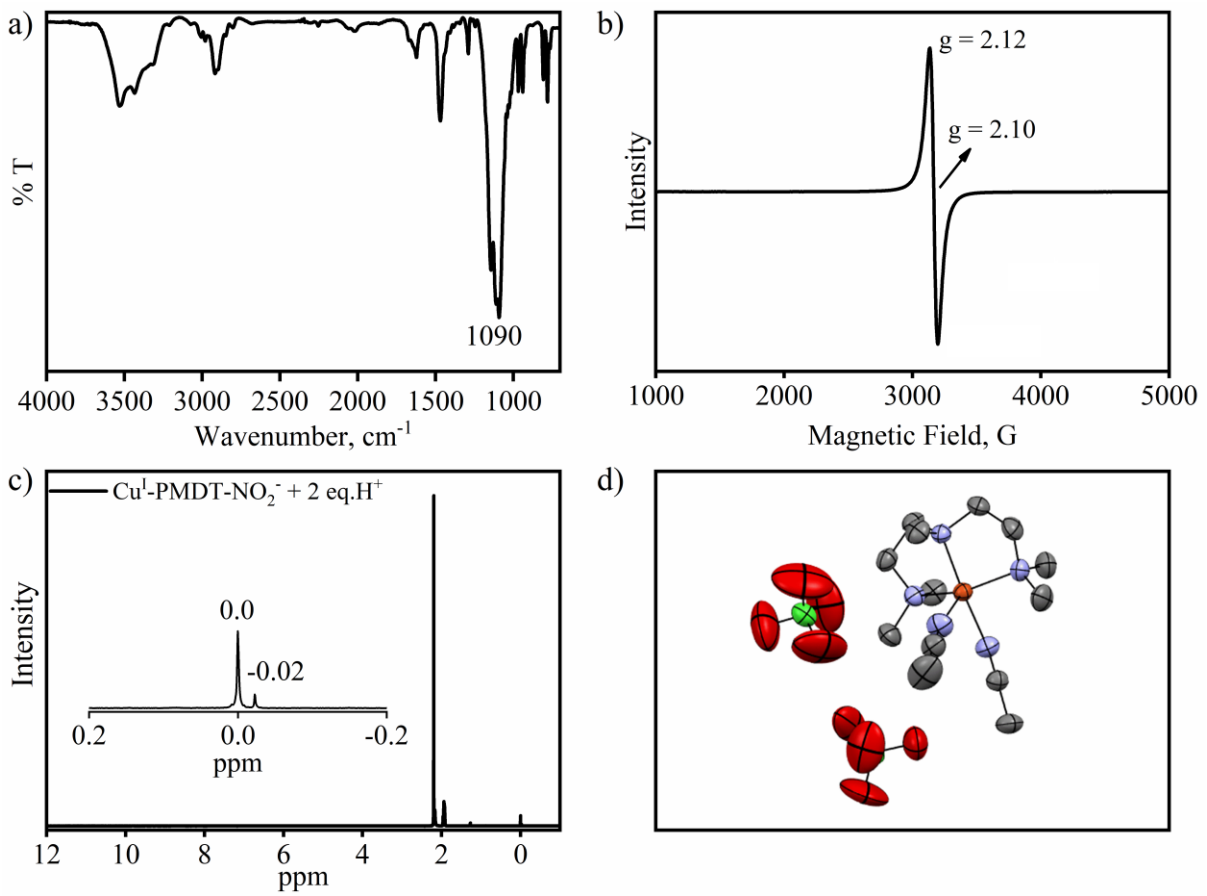

Figure S4. (a) FT-IR spectrum of **3** recorded in a KBr pellet at 298 K. Absence of a peak at 1270 cm^{-1}. (b) EPR spectrum of **3** obtained from the reaction of **2** with two equivalents of H^+ performed at 233K. (c) Evans' method ^{1}H-NMR (400 MHz) spectra of **3** isolated from the reaction of **2** with two equivalents of H^+. (d) Displacement ellipsoid plots (50% probability level) of **3** obtained from the reaction of **2** with two equivalents of H^+. Hydrogen atoms are removed for better clarity. (Orange: Cu, Blue: N, Grey: C, Green: Cl, Red: O)

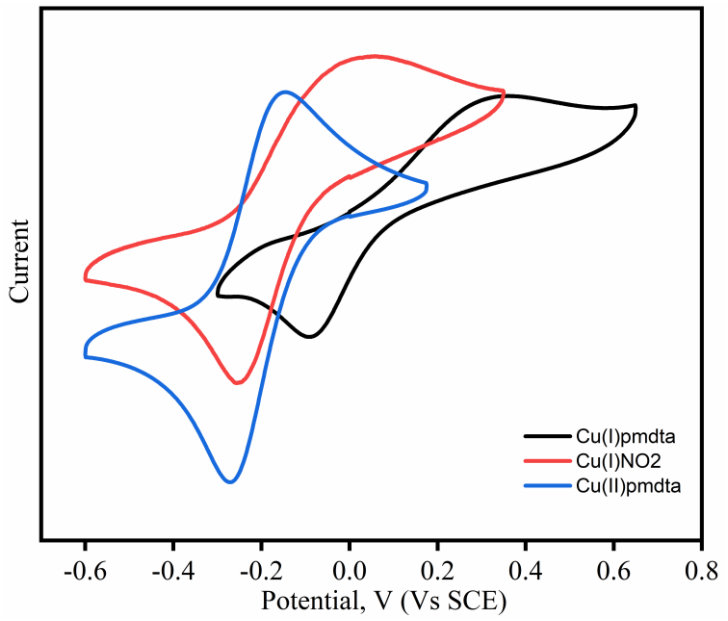

Figure S5. Cyclic Voltammograms of complexes **1**, **2**, and **3** CH_3CN/0.1 M Bu_4NPF_6 at 298 K under Ar.

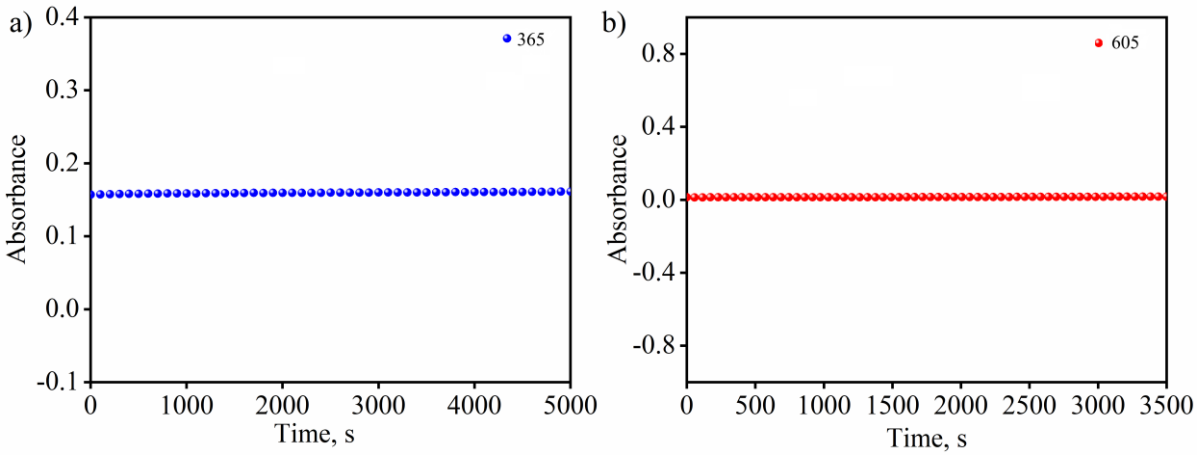

Figure S6. (a) Time course for the spectral changes of **2** (0.5 mM) (blue circles) in CH_3CN under Ar. (b) Time course for the spectral changes of **1** (red circles) in the presence of H^+ in CH_3CN under Ar.

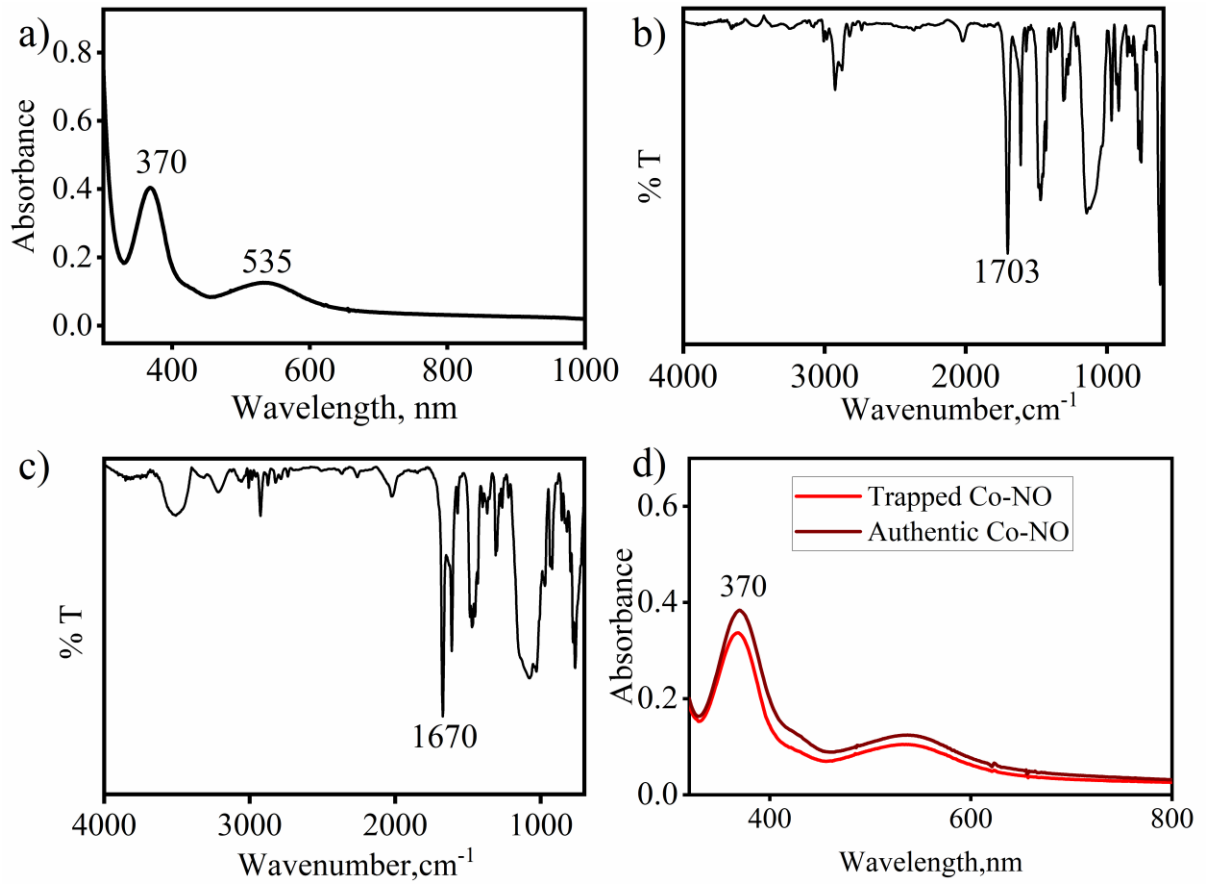

Figure S7. (a) Electronic absorption spectrum of $\{CoNO\}^8$ (showing the characteristic peaks at 370 nm and 535 nm) formed in the reaction of **2** (40 mM) + $HClO_4$ (two equivalents) + [(12-TMC)$Co^{II}(CH_3CN)$](BF_4) (40 mM) (b) FT-IR spectrum of $\{Co^{14}NO\}^8$ in a KBr pellet at 298 K isolated from the reaction **2**-$^{14}NO_2^-$ (40 mM) + $HClO_4$ (two equivalents) + [(12-TMC)$Co^{II}(CH_3CN)$](BF_4) (40 mM). The spectrum showed a peak for $\{Co^{14}NO\}^8$ (at 1703 cm^{-1}). (c) FT-IR spectrum of $\{Co^{15}NO\}^8$ in a KBr pellet at 298 K isolated from the reaction **2**-$^{15}NO_2^-$ (40 mM) + $HClO_4$ (two equivalents) + [(12-TMC)$Co^{II}(CH_3CN)$](BF_4) (40 mM). The spectrum showed a peak for $\{Co^{15}NO\}^8$ (at 1670 cm^{-1}). (d) Comparison of electronic absorption spectra of $\{Co\text{-}NO\}^8$ generated in situ reaction of **2** (0.5 mM) + two equivalents H^+ + [(12-TMC)$Co^{II}(NCCH_3)]^{2+}$ (0.5 mM) (red colour) and authentic $[Co(12\text{-}TMC)(NO)]^{2+}$ (Wine colour) performed in CH_3CN. This NO-trapping reaction was performed under Ar to prevent NO from reacting with O_2.

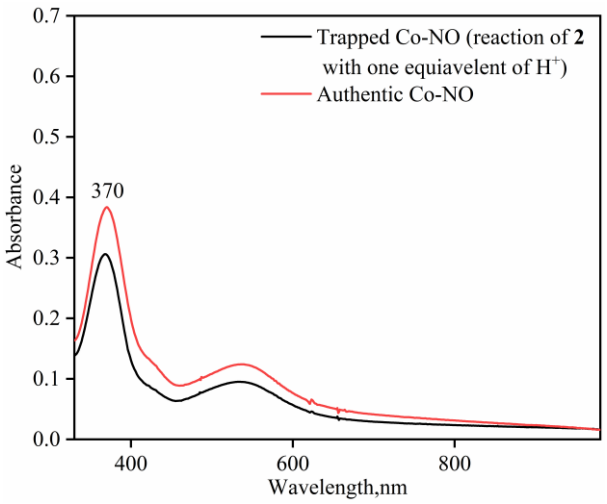

Figure S8. Comparison of electronic absorption spectra of {Co-NO}^{8} generated in-situ reaction of **2** (0.5 mM) + one equivalents H^+ + $[(12\text{-TMC})Co^{II}(NCCH_3)]^{2+}$ (black colour) and authentic $[Co(12\text{-TMC})(NO)]^{2+}$ (red colour) in CH_3CN.

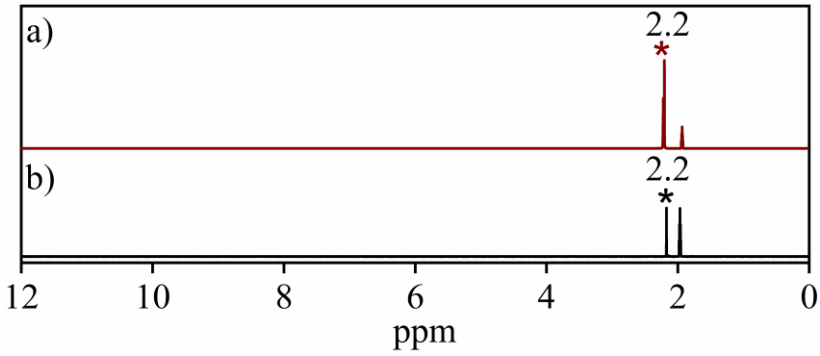

Figure S9. (a) ^{1}H-NMR (400 MHz) spectrum of reaction of **2** (5 mM) with two equivalents of H^{+}, recorded in CD_3CN at 298 K under Ar, showed the appearance of a signal at ~2.2 ppm, which corresponds to the formation of H_2O in the nitrite reduction reaction (b) ^{1}H-NMR (400 MHz) spectrum of **3 (**5 mM) recorded in CD_3CN at 298 K under Ar, where the appearance of the signal at ~2.2 ppm corresponds to H_2O present in complex **3**, showing residual solvent water.

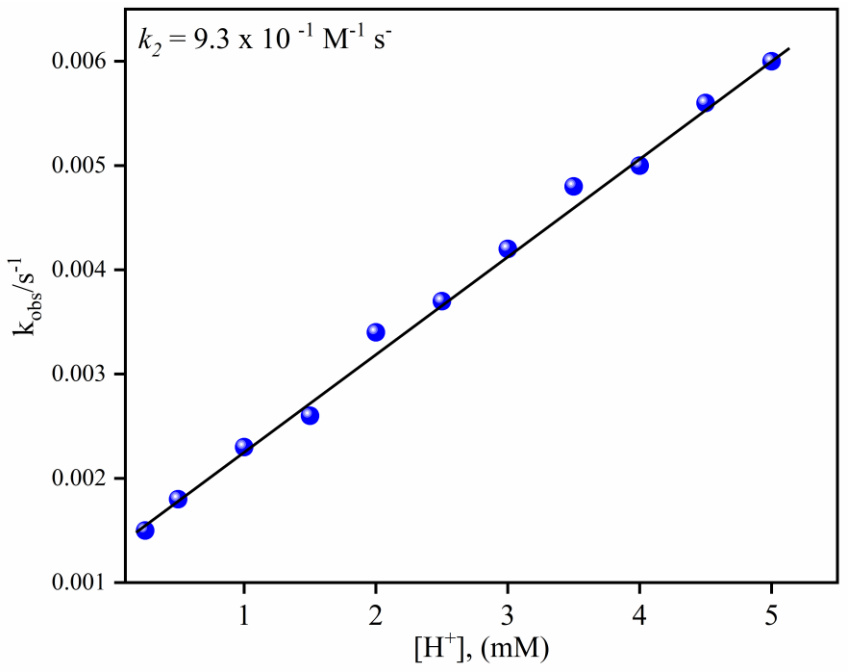

Figure S10. Plots of pseudo-first-order rate constant (k_{obs}) for the formation of **2** against the varying concentration of H^+ (0.5, 1, 1.5, 2, 2.5, 3, 3.5, 4, 4.5, 5 equivalents of H^+).

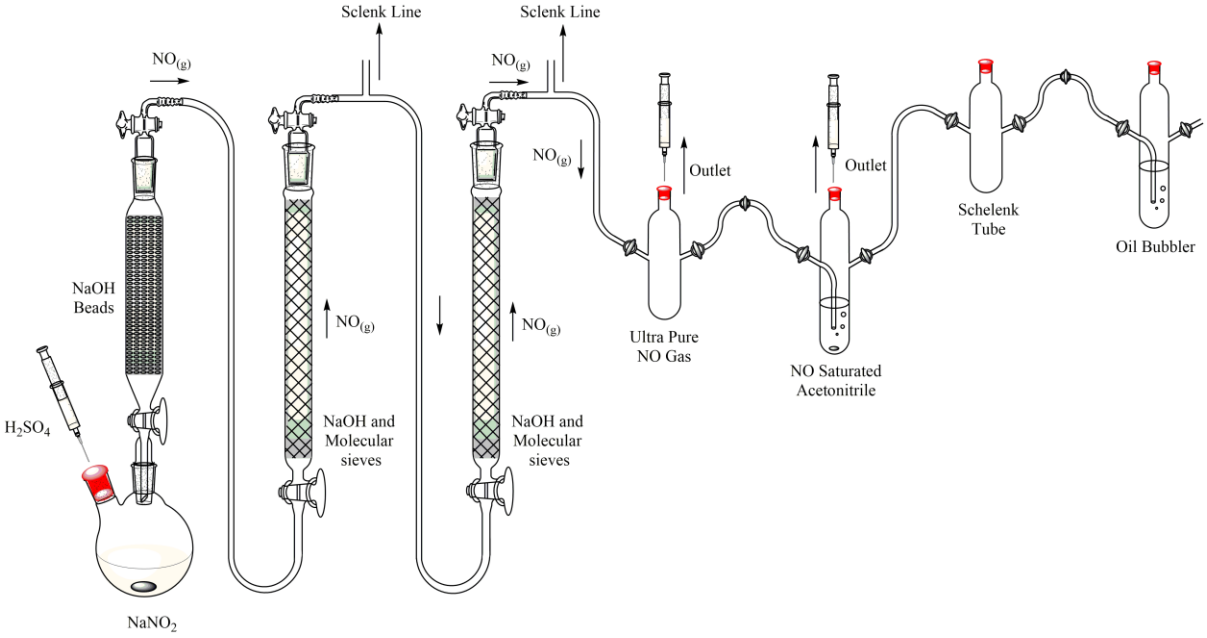

Figure S11. Schematic diagram showing the generation and purification setup for NO.

Optimized geometries of the {Cu-OH}$^{+}$ cation (M06/Def2-TZVP, acetonitrile)

Cu	-0.004072000	-0.434122000	-0.546960000
N	1.907651000	-0.463436000	0.322301000
N	0.005795000	1.582968000	-0.160727000
N	-1.907939000	-0.447015000	0.333390000
C	-2.090443000	-1.676451000	1.098897000
H	-1.270427000	-1.793626000	1.810115000
H	-3.039893000	-1.651483000	1.650765000
C	1.211730000	1.869905000	0.656608000
H	1.963636000	2.311514000	0.000564000
C	-2.965138000	-0.323048000	-0.666153000
H	-2.934991000	-1.192038000	-1.324164000
H	-3.950354000	-0.272502000	-0.183290000
H	-2.824170000	0.571886000	-1.272633000
C	2.148045000	-1.731476000	1.007714000
H	2.245147000	-2.533643000	0.275688000
C	0.086000000	2.264074000	-1.460700000
H	-0.773817000	1.984272000	-2.070711000
H	0.996611000	1.961007000	-1.979055000
C	1.761335000	0.622527000	1.303698000
H	1.080814000	0.264069000	2.081454000
H	2.727621000	0.838392000	1.780791000
C	2.983286000	-0.205374000	-0.632948000
H	3.028851000	-1.024777000	-1.351729000
H	2.805073000	0.721453000	-1.177982000
H	3.071703000	-1.680513000	1.599293000
H	1.312108000	-1.958575000	1.671383000
H	3.949163000	-0.132831000	-0.115410000
H	0.981891000	2.614840000	1.422908000
H	0.093532000	3.353008000	-1.333304000
C	-1.271047000	1.912902000	0.515701000
H	-1.128482000	2.739680000	1.217254000
H	-1.969995000	2.261213000	-0.246440000
C	-1.842175000	0.715554000	1.230782000
H	-2.839201000	0.950135000	1.628691000
H	-1.207833000	0.440999000	2.078396000
H	-2.090680000	-2.528227000	0.419645000
O	-0.128552000	-2.079685000	-1.368612000
H	0.752088000	-2.416551000	-1.557829000